Statistics of S_{xy} Estimates

M. H. FREILICH

Jet Propulsion Laboratory, California Institute of Technology, Pasadena, CA 91109

S. S. PAWKA*

Center for Coastal Studies, Scripps Institution of Oceanography, La Jolla, CA 92093

(Manuscript received 19 March 1986, in final form 20 May 1987)

ABSTRACT

The statistics of S_{xy} estimates derived from orthogonal-component measurements are examined. Based on results of Goodman, the probability density function (pdf) for $S_{xy}(f)$ estimates is derived, and a closed-form solution for arbitrary moments of the distribution is obtained. Characteristic functions are used to derive the exact pdf of S_{xy}^{tot}. In practice, a simple Gaussian approximation is found to be highly accurate even for relatively few degrees of freedom. Implications for experiment design are discussed, and a maximum likelihood estimator for a posteriori estimation is outlined.

1. Introduction

Wave-induced fluxes of momentum (Longuet-Higgins and Stewart, 1964) play a crucial role in many nearshore processes. In particular, the onshore flux of longshore momentum has been related to both longshore currents in the surf zone (Bowen, 1969; Longuet-Higgins, 1970a,b) and longshore transport of sediment near the beach (e.g., Komar and Inman, 1970).

In order to test dynamical models, accurate measurements of both the wave-induced fluxes and the sediment transport or mean currents are necessary. Equally necessary, however, is an understanding of the statistical properties of quantities derived from the field measurements. Such statistical knowledge is required in order to design meaningful data acquisition strategies, and to interpret properly the significance of correlations between experimental data and model predictions.

It is the purpose of this paper to investigate the statistics of wave-induced onshore fluxes of longshore momentum inferred from measurements of horizontal currents or sea-surface slopes.

The onshore flux of longshore momentum, S_{xy}, is defined (Longuet-Higgins and Stewart, 1964) as

$$S_{xy} = \left\langle \int_{-h}^{\eta} uv dz \right\rangle, \tag{1.1}$$

where $\eta(t)$ is the sea-surface elevation, $h(x)$ is the depth, $u(x, z, t)$ and $v(x, z, t)$ are the onshore and longshore components of velocity, z is the vertical coordinate measured upward from the undisturbed sea surface, and $\langle \cdot \rangle$ represents an average over all possible realizations of the wave field. If the wave field is nearly linear, Eq. (1.1) can be rewritten, correct to second order (Longuet-Higgins, 1970a), as

$$S_{xy} = \int_{-h}^{0} \langle uv \rangle dz. \tag{1.2}$$

Further assumptions regarding the Gaussian nature of the surface elevation field (Kinsman, 1965) yield the well-known relation (e.g., Pawka et al., 1983)

$$S_{xy} = \int_0^\infty gn(f) \int_0^{2\pi} \Phi(f, \theta) \sin\theta \cos\theta d\theta df, \tag{1.3}$$

where $n(f)$ is the ratio between the group speed and the phase speed for linear, irrotational waves, $\Phi(f, \theta)$ is the (one-sided) frequency–directional spectrum of sea-surface elevation, and the density of water has been set equal to 1.

Consistent with the assumption of linearity, an S_{xy} density, $S_{xy}(f)$, can be defined (Pawka et al., 1983):

$$S_{xy}(f) = gn(f) \int_0^{2\pi} \Phi(f, \theta) \sin\theta \cos\theta d\theta, \tag{1.4a}$$

such that

$$S_{xy} = \int_0^\infty S_{xy}(f) df. \tag{1.4b}$$

Knowledge of the full frequency–directional spectrum is not necessary for the calculation of $S_{xy}(f)$. As suggested by the form of (1.2), Pawka et al. (1983) show that $S_{xy}(f)$ can be calculated from simultaneous measurements of horizontal current components:

* Deceased.

$$S_{xy}(f) = n(f)\left(\frac{2\pi f}{gk}\right)^2\left[\frac{\cosh(kh)}{\cosh(kz')}\right]^2\Lambda_{uv}(f), \quad (1.5)$$

where k is the magnitude of the wavenumber, z' is the distance from the bottom at which the measurements were made, and $\Lambda_{uv}(f)$ is the cross-spectral density of the cross-shore (u) and alongshore (v) velocity components. Similarly, Higgins et al. (1981) give

$$S_{xy}(f) = (g/k^2)\Lambda_{\eta_x\eta_y}(f), \quad (1.6)$$

where η_x and η_y are cross-shore and alongshore components of surface slope. We note that although the cross-spectrum Λ in general is complex, the linearity of the wave field requires that

$$\mathrm{Im}[\Lambda_{uv}(f)] = \mathrm{Im}[\Lambda_{\eta_x\eta_y}(f)] \equiv 0.$$

If knowledge of the *true* values of $\langle uv\rangle$, $\Phi(f, \theta)$, $\Lambda_{uv}(f)$, or $\Lambda_{\eta_x\eta_y}$ were available from measurements, calculations of $S_{xy}(f)$ would be trivial. In fact, however, the mean product, frequency-directional spectral density, or cross-spectral densities can only be *estimated* from finite sets of measurements. Pawka et al. (1983) discuss various methods for combining sea-surface elevation measurements from a linear array of wave gages in order to estimate $\Phi(f, \theta)$ and the crucial moment of (1.3). Seymour and Higgins (1977), Higgins et al. (1981), and Pawka et al. (1983) utilize estimates of orthogonal component cospectra for the calculation of $S_{xy}(f)$. However, there has been little discussion in the literature of the *statistics* of the spectral or cospectral estimates, and there has been no discussion of the statistics of estimates of $S_{xy}(f)$ and S_{xy}. The present paper addresses this issue for the case of estimates derived from orthogonal-component measurements.

In section 2, we examine the joint statistics of auto- and cross-spectral estimates, drawing on the pioneering work of Goodman (1957, 1963). We discuss the implications of the statistical variability of these estimates on estimation of $S_{xy}(f)$. Statistics of estimates of S_{xy} are derived in section 3. Results from sections 2 and 3 are discussed, in the context of experimental design, in section 4. Section 5 illustrates the use of maximum likelihood techniques for estimating *true* $S_{xy}(f)$ values (and their uncertainties) after data has been collected. Conclusions are summarized in section 6.

2. Statistics of $\hat{S}_{xy}(f)$

In this section we examine the probability density function (pdf) for estimates of $S_{xy}(f)$ calculated from orthogonal component (slope arrays or horizontal current meters) measurement systems, drawing heavily on the results of Goodman (1957, 1963) and Pawka (1982). Throughout this paper, a caret above a symbol will denote an estimate of the quantity. Equations (1.5) and (1.6) show that estimates $\hat{S}_{xy}(f)$ are directly proportional to estimates, $\hat{C}(f)$, of the frequency cospectrum between orthogonal components of surface slope or horizontal velocity. The statistics of $\hat{S}_{xy}(f)$ are thus intimately related to the statistics of cross-spectral estimates. Goodman (1957, 1963) was the first to derive rigorously the relevant cross-spectrum statistics (see also Borgman, 1976); in the present article we use Goodman's major results without derivation.

We define $u(t)$, $v(t)$ $(0 \leq t \leq T)$ to be finite-length, orthogonal-component time series as, for instance, would be measured by a dual-axis current meter outside the break zone. The time series have discrete, complex Fourier transforms $U(f_i)$ and $V(f_i)$, $f_i = i/T$. If it is assumed that the wave field is linear with Gaussian sea-surface elevations, then the real and imaginary parts of $U(f_i)$ and $V(f_i)$ are four-variate normally distributed.

Given n independent realizations of the time series $u(t)$ and $v(t)$, sample auto- and cross-spectral quantities can be defined as in Table 1 (note that unless specifically required, explicit references to the frequency index f_i are dropped in Table 1 and the following discussion). Goodman derives the joint pdf of the auto- and cross-spectral estimates $\hat{A}$, $\hat{B}$, $\hat{C}$, $\hat{D}$:

$$p(\hat{A}, \hat{B}, \hat{C}, \hat{D}) = \left[\frac{n^{2n}}{\pi\Gamma(n)\Gamma(n-1)}\right][AB\delta]^{-n}[\hat{A}\hat{B} - \hat{C}^2 - \hat{D}^2]^{n-2} \times \exp\left\{\frac{n}{\delta}\left[\frac{2(\hat{C}^2+\hat{D}^2)}{AB} - \frac{\hat{A}}{A} - \frac{\hat{B}}{B}\right]\right\}, \quad (2.1)$$

where

$$\delta \equiv 1 - \alpha^2 - \beta^2 \geq 0, \quad (2.2)$$

and

$$p(\hat{A}, \hat{B}, \hat{C}, \hat{D}) = 0 \quad \text{for} \quad \delta < 0.$$

In this section, we restrict our attention to the statistics of the cospectrum estimate $\hat{C}$. Thus, following Goodman, standard techniques can be used to integrate (2.1) with respect to $\hat{A}$, $\hat{B}$ and $\hat{D}$ to yield

$$p(\hat{C}) = \int_0^\infty d\hat{A}\int_0^\infty d\hat{B}\int_0^\infty d\hat{D}\, p(\hat{A}, \hat{B}, \hat{C}, \hat{D}) = \left[\frac{2}{\sqrt{\pi}\Gamma(n)}\right]\left[\frac{n^{n+1/2}}{\delta^{1/2}(AB)^{n/2+1/4}(1-\beta^2)^{n/2-1/4}}\right][|\hat{C}|^{n-1/2}] \times \exp\left\{\frac{2n\alpha}{\delta\sqrt{AB}}\hat{C}\right\}\left[K_{n-1/2}\left(\frac{2n}{\delta\sqrt{AB}}|\hat{C}|\sqrt{1-\beta^2}\right)\right], \quad (2.3)$$

where $K_{n-1/2}(\cdot)$ is the modified Bessel function of the third kind (Abramowitz and Stegun, 1970).

In terms of the normalized variable $\tilde{C} \equiv \hat{C}/C$, (2.3) can be written

$$p(\tilde{C}) = \left[\frac{n^{n+1/2}}{\sqrt{\pi}\Gamma(n)}\right]\left[\frac{2|\alpha|^{n+1/2}}{\delta^{1/2}(1-\beta^2)^{n/2-1/4}}\right]|\tilde{C}|^{n-1/2} \times \exp\left\{\frac{2n\alpha^2}{\delta}\tilde{C}\right\}\left[K_{n-1/2}\left(\frac{2n}{\delta}|\alpha|\sqrt{1-\beta^2}|\tilde{C}|\right)\right]. \quad (2.4)$$

In all of the following, we set $\beta = 0$, corresponding

TABLE 1. Definitions of sample estimates and true auto- and cross-spectral values. Throughout the paper, carets over quantities represent sample estimates.

Symbol	Definition	Comments
$u_j(t), v_j(t)$		Finite-length time series from orthogonal component measurements
$\hat{U}_j(f), \hat{V}_j(f)$	$\begin{Bmatrix}\hat{U}_j(f)\\ \hat{V}_j(f)\end{Bmatrix} = \int_0^T \begin{Bmatrix}u_j(t)\\ v_j(t)\end{Bmatrix} e^{-2\pi i f t} dt$	Complex Fourier coefficients
$\hat{A}, \hat{B}$	$\begin{Bmatrix}\hat{A}\\ \hat{B}\end{Bmatrix} = \frac{1}{2n\Delta} \sum_{j=1}^{n} \begin{Bmatrix}\hat{U}_j \hat{U}_j^*\\ \hat{V}_j \hat{V}_j^*\end{Bmatrix}$	Auto-spectral densities
$\hat{\Lambda}$	$\frac{1}{2n\Delta f} \sum_{j=1}^{n} \hat{U}_j^* \hat{V}_j$	Complex cross-spectral density
$\hat{C}$	$\mathrm{Re}[\hat{\Lambda}]$	Co-spectral density
$\hat{D}$	$\mathrm{Im}[\hat{\Lambda}]$	Quad-spectral density
$\hat{\alpha}$	$\hat{C}/\sqrt{\hat{A}\hat{B}}$	Normalized co-spectral density
$\hat{\beta}$	$\hat{D}/\sqrt{\hat{A}\hat{B}}$	Normalized quad-spectral density
A, B		True autospectral densities
Λ		True cross-spectral density
C	$\mathrm{Re}[\Lambda]$	True co-spectral density
D	$\mathrm{Im}[\Lambda]$	True quad-spectral density
α	$C/\sqrt{AB}$	True normalized co-spectral density
β	$D/\sqrt{AB}$	True normalized quad-spectral density

to the assumption of a linear wave field. Plots of $p(\tilde{C})$ for various values of n and α are shown in Fig. 1.

For purposes of comparison, we also present the (chi-squared) pdf for normalized autospectral estimates $\tilde{A} = \hat{A}/A$:

$$p(\tilde{A}) = \begin{cases} \dfrac{n^n \tilde{A}^{n-1} \exp\{-n\tilde{A}\}}{\Gamma(n)}, & \text{for} \quad \tilde{A} \geq 0, \\ 0, & \text{otherwise.} \end{cases} \tag{2.5}$$

Comparison of (2.4) with (2.5) reveals several important differences. First, while $p(\tilde{A}) > 0$ only for $\tilde{A} > 0$ (reflecting the fact that auto-spectral estimates are always non-negative), $p(\tilde{C}) > 0$ for both positive and negative values of $\tilde{C}$. There is thus a nonzero probability that the *sign* of the cospectrum estimate $\hat{C}$ differs from the sign of the true cospectral value C. In terms of $S_{xy}(f)$ estimates derived from $\hat{C}$, there is a nonzero probability that the *direction* of the momentum flux as estimated from measurements will be opposite to that of the true momentum flux. Figure 2 shows the probability, as a function of n and α, of estimating an incorrect sign for the momentum flux. For large values of $|\alpha|$ (i.e., $C \to \sqrt{AB}$, corresponding to a near-plane wave), the integrated probability for $\tilde{C} < 0$ is very small for all n. This is in consequence of the fact that, for a plane wave, the orthogonal components are perfectly coherent and $p(\tilde{C}; \alpha = 1)$ reduces to a distribution proportional to a χ^2_{2n} distribution. The integrated probability of $\tilde{C} < 0$ is largest for small $|\alpha|$ and small n.

Second, knowledge of the *true value*, α, is necessary in order to define the distribution of the normalized cospectrum $\tilde{C}$, while such is not the case for normalized autospectral values. As $2n\tilde{A}$ is χ^2_{2n} distributed, the distribution of $\tilde{A}$ is completely specified by knowledge of $2n$, the equivalent degrees of freedom of the estimate $\tilde{A}$. That this is not true for the case of $\tilde{C}$ is evident by the explicit appearance of α in (2.4). Thus, the distribution of sample normalized cospectrum estimates is a function not only of the sampling parameter n (which can be controlled by the experimenter), but also of the true cospectrum. (For a related discussion regarding coherence and phase, see Jenkins and Watts, 1968.)

Finally, as can be seen in Fig. 1, $p(\tilde{C})$ is broader than $p(\tilde{A})$ for all values of $|\alpha|$. Since as $|\alpha|$ approaches 1 (2.4) approaches (2.5), it is clear that for fixed n, the variability of normalized cospectral estimates (and hence, momentum flux density estimates) is always larger than the variability of auto-spectral estimates. This is especially true for small values of $|\alpha|$.

The variability of normalized cospectral [and $S_{xy}(f)$] estimates can be examined more quantitatively by investigating the low-order moments of distributions similar to (2.3), as suggested by Pawka (1982). Since $S_{xy}(f)$ is directly proportional to $C(f)$,

$$p[\hat{S}_{xy}(f)/S_{xy}(f)] = p(\hat{C}/C) = p(\tilde{C}). \tag{2.6}$$

We define the mth moment of the distribution in the usual fashion as

$$I_m(\tilde{C}; n, \alpha) \equiv \int_{-\infty}^{\infty} \tilde{C}^m p(\tilde{C}) d\tilde{C}. \tag{2.7}$$

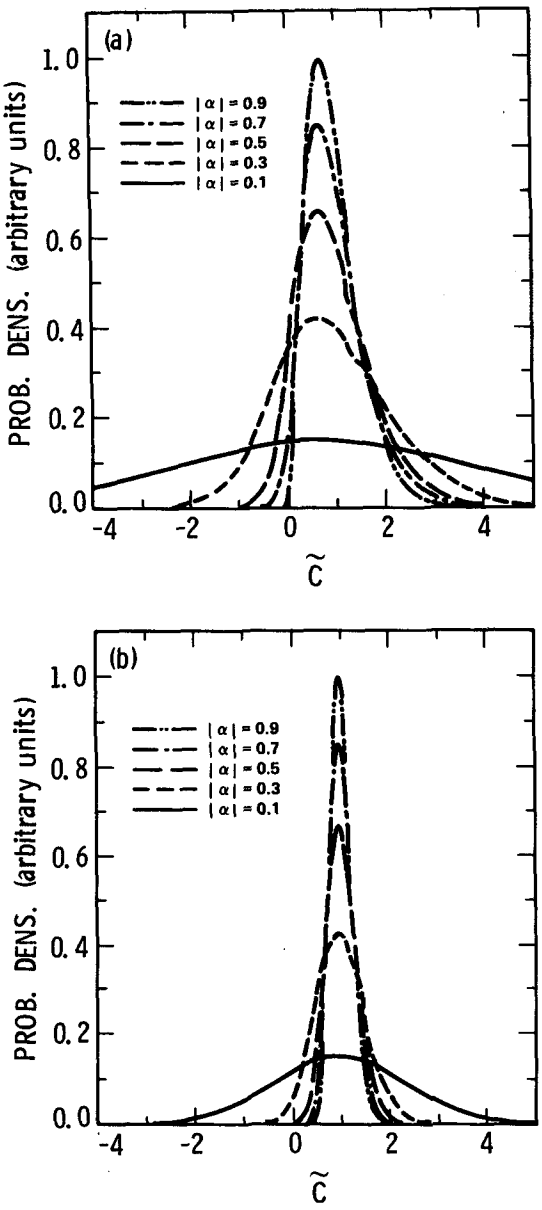

FIG. 1. Probability density function of $\tilde{C}$ for $|\alpha| = 0.1, 0.3, 0.5, 0.7$ and 0.9. (a) $n = 4$; (b) $n = 100$. In each plot, curves are normalized such that the maximum value for $|\alpha| = 0.9$ is 1.

Substitution of (2.4) and the series definition of the modified Bessel function of the third kind (Abramowitz and Stegun, 1970) into (2.7), followed by straightforward (and rather tedious) integration yields

$$I_m(\tilde{C}; n, \alpha) = \frac{\delta^{n+m}}{(n\alpha)^m (n-1)!} \sum_{k=0}^{n-1} \left\{ \frac{(n-1+k)!(n-1-k+m)!}{2^{n+k+m} k!(n-1-k)!} \times [(1-\alpha)^{k-n-m} + (-1)^m (1+\alpha)^{k-n-m}] \right\}, \quad (2.8)$$

valid for $0 < |\alpha| < 1$ and for integer values of n. Equation (2.8) is thus an *exact, closed-form solution* for the moments of the normalized cospectrum and is easily evaluated numerically. It can be shown (by induction) that for the special case $m = 2$, (2.8) reduces to the well-known form given, for example, by Borgman et al. (1982).

Simple manipulations of (2.7) and the definition of $\tilde{C}$ yield

$$I_m = E[\tilde{C}^m] = E[\hat{C}^m]/C^m. \quad (2.9)$$

Physically, I_1 corresponds to the normalized mean of the cospectral estimate $\hat{C}$, which is also the mean of the normalized estimate $\hat{S}_{xy}(f)/S_{xy}(f) = \hat{C}/C$. Likewise, $\text{var}[\tilde{C}] = I_2 - I_1^2$ corresponds to the normalized variance of $\hat{C}$, which is also the variance of the quantity $[\hat{S}_{xy}(f)/S_{xy}(f)]$.

From the definition of C (Table 1) and the fact that the real and imaginary parts of the Fourier coefficients $U(f)$ and $V(f)$ are four-variate normally distributed, Goodman (1957) shows that

$$I_1(\tilde{C}; n, \alpha) = 1. \quad (2.10)$$

[This result can also be obtained by evaluating (2.8) directly.] The variable $\hat{C}$ is thus an unbiased estimator of the true cospectrum C.

Figure 3 shows the normalized variance of $\hat{C}$ as a function of the parameters n and α. For fixed n, $\text{var}[\tilde{C}; n, \alpha]$ decreases with increasing α, while for fixed α, $\text{var}[\tilde{C}; n, \alpha]$ decreases with increasing n. Although $\text{var}[C; n, \alpha]$ decreases rapidly with n for n small, it is much less sensitive to n for n large. In fact, for $n > 20$,

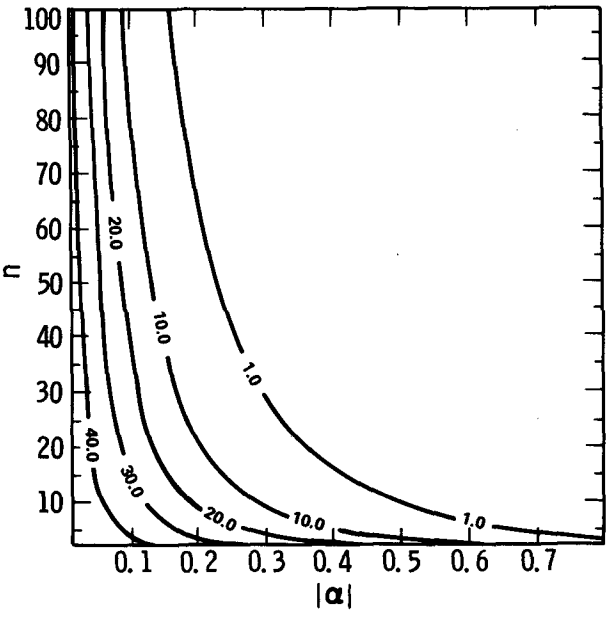

FIG. 2. Contour plot of $\int_{-\infty}^{0} p[\tilde{S}_{xy}(f)]d\tilde{S}_{xy}(f)$ as a function of $|\alpha|$ and n. Contours represent probability (in percent) that an estimate of $S_{xy}(f)$ will have an incorrect sign.

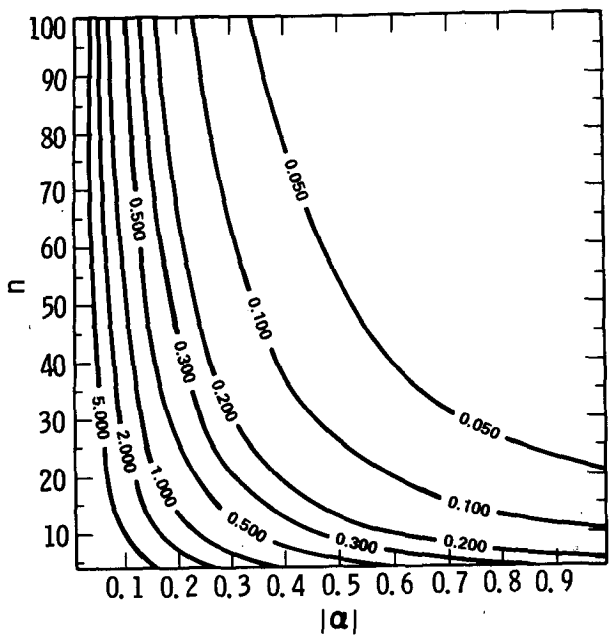

FIG. 3. Variance of $\tilde{C}$ [or $\hat{S}_{xy}(f)$] as a function of $|\alpha|$ and n.

var[$\tilde{C}$; n, α] is nearly independent of n for $\alpha = 0.9$, while for $\alpha = 0.1$, var[$\tilde{C}$; n, α] is nearly insensitive to n for $n > 40$. Pawka (1982) gives examples (for selected values of α) of the dependence of normalized skewness and kurtosis on the degrees of freedom $2n$.

3. Statistics of $\hat{S}_{xy}^{\text{tot}}$

The total onshore flux of longshore momentum, S_{xy}^{tot}, is obtained by integrating $S_{xy}(f)$ over frequency as in (1.4b). In the previous section, we examined the statistics of the density estimator $\hat{S}_{xy}(f)$ defined in Table 1. In this section, we present both exact and approximate methods for evaluating the statistics of $\hat{S}_{xy}^{\text{tot}}$.

The estimator $\hat{S}_{xy}^{\text{tot}}$ is defined as the sum of the estimates $\hat{S}_{xy}(f)$ over the frequency range of interest

$$\hat{S}_{xy}^{\text{tot}} \equiv (\Delta f) \sum_j \hat{S}_{xy}(f_j). \tag{3.1}$$

As the estimators $\hat{S}_{xy}(f)$ are themselves random variables, $\hat{S}_{xy}^{\text{tot}}$ is a random variable composed of the sum of other random variables. One can derive the pdf of $\hat{S}_{xy}^{\text{tot}}$ given the pdf of the variables $\hat{S}_{xy}(f)$ through the use of characteristic functions. If the random variable $\hat{S}_{xy}(f)$ can take values x ($-\infty \leq x \leq \infty$), its characteristic function is defined as

$$\phi_{\hat{S}_{xy}(f_j)}(u) = E[\exp\{iu\hat{S}_{xy}(f_j)\}]$$
$$= \int_{-\infty}^{\infty} \exp\{iu\hat{S}_{xy}(f_j)\} d\{p[\hat{S}_{xy}(f_j)]\}, \tag{3.2}$$

where $p[\hat{S}_{xy}(f_j)]$ is the pdf of $\hat{S}_{xy}(f_j)$. The characteristic function is thus the Fourier transform of the pdf. Using (3.1),

$$\phi_{\hat{S}_{xy}^{\text{tot}}}(u) = \phi_{\hat{S}_{xy}(f_1)}(u) \cdot \phi_{\hat{S}_{xy}(f_2)}(u) \cdot \cdots \phi_{\hat{S}_{xy}(f_n)}(u)$$
$$= \prod_j \phi_{\hat{S}_{xy}(f_j)}(u), \tag{3.3}$$

where the product over j spans the same range as the sum in (3.1). Since products of Fourier transforms are equivalent to convolutions of the original (untransformed) variables, (3.3) may be inverse transformed to yield

$$p(\hat{S}_{xy}^{\text{tot}}) = p[\hat{S}_{xy}(f_1)] * p[\hat{S}_{xy}(f_2)] * \cdots * p[\hat{S}_{xy}(f_n)], \tag{3.4}$$

where $*$ indicates convolution. Goodman (1957) gives the characteristic function for the normalized cospectrum $\tilde{C}$ as

$$\phi_{\tilde{C}}(\theta_{\tilde{C}}) = \delta^n \left[1 - \beta^2 - \left(\alpha + i\frac{\delta}{2n\alpha}\theta_{\tilde{C}}\right)^2\right]^{-n}; \tag{3.5a}$$

in terms of $\hat{S}_{xy}(f_j)$ (setting $\beta = 0$),

$$\phi_{\hat{S}_{xy}(f_j)}[\theta_{\hat{S}_{xy}(f_j)}] = \delta^n \{1 - [\alpha + i\rho\theta_{\hat{S}_{xy}(f_j)}]^2\}^{-n}, \tag{3.5b}$$

where the proportionality constant $\rho(f_j)$ is given by

$$\rho(f_j) = \frac{\delta S_{xy}(f_j)}{2n\alpha(f_j)}. \tag{3.5c}$$

Equations (1.5) and (1.6) can likewise be used to relate (3.5b) directly to a characteristic function for $\hat{S}_{xy}(f_j)$ based on the Fourier transform pair of the measured cospectrum from an orthogonal component measuring system.

Substitution of (3.5b) into (3.3), followed by direct Fourier transformation, yields the pdf of $\hat{S}_{xy}^{\text{tot}}$. While in principle the result could probably be derived analytically, in practice (3.3) and the resulting (discrete) Fourier transform are evaluated numerically when high accuracy is needed.

Analysis of the pdf given by (2.4), however, indicates that an accurate simplification of the exact formulae can be made. Specifically, as shown in section 2, $p[\hat{S}_{xy}(f_j)]$ is proportional to $p(\tilde{C})$ given by (2.4). If $p(\tilde{C})$, and hence $p[S_{xy}(f_j)]$, could be accurately approximated by a normal distribution function, then the individual characteristic functions (3.5b) would be Gaussian (since the Fourier transform of a Gaussian is itself a Gaussian). Furthermore, the product, (3.3) would *also* be Gaussian, and hence its transform, $p(\hat{S}_{xy}^{\text{tot}})$, would be Gaussian.

Table 1 shows that $\hat{C}$ [and $\hat{S}_{xy}(f_j)$] is a sum of independent (and like-distributed) random variables. Thus, for large n, the central limit theorem assures that $p(\hat{C})$ must be a normal distribution (Jenkins and Watts, 1968; Long, 1980). However, examination of Fig. 1a suggests that the normal approximation may be valid, even for small n, over a wide range of $|\alpha|$. We quantitatively tested the limits of validity of the normal assumption by using the nonparametric χ^2 test (Haub-

rich, 1965; Bendat and Piersoll, 1971). For $0 \leq |\alpha| \leq 1$ and $4 < n < 25$ (for $n > 25$, the central limit theorem holds for all $|\alpha|$), $p(\tilde{C})$ was calculated using (2.4), and fit to a Gaussian in a least-squares manner. Normalized square deviations between $p(\tilde{C})$ and the best-fit Gaussian were calculated for 400 equally spaced values of $\tilde{C}$ [chosen such that $p(\tilde{C}_{low}) = p(\tilde{C}_{high}) = 10^{-6}p(\tilde{C}_{max})$ where $\tilde{C}_{max}$ corresponds to the maximum of the pdf] at each value of n, $|\alpha|$. The sum of the normalized square deviations is the χ^2 statistic. Figure 4, constructed from the field of χ^2 statistics in $(n, |\alpha|)$ space, shows the contour corresponding to the 95% significance level for the validity of the normal approximation. Except for the hatched region in Fig. 4 corresponding to n small and $|\alpha|$ near 1, the approximation is highly accurate.

Using the normal approximation, (3.3) can be rewritten as

$$\phi_{\hat{S}_{xy}^{tot}}(\theta) = \exp\{-2\pi i \sum_j S_{0_j}\} \exp\{-\tfrac{1}{2}[\sum_j (S_{0_j}\sigma_j)^2\theta^2]\}, \tag{3.6}$$

where $S_{0_j} = S_{xy}(f_j)$, and $\sigma_j^2 = I_2(\tilde{C}; n, \alpha) - I_1^2(\tilde{C}; n, \alpha)$ as given by (2.8). Doing the inverse transformation analytically, (3.4) becomes

$$p(\hat{S}_{xy}^{tot}) = [2\pi \sum_j (S_{0_j}\sigma_j)^2]^{-1/2} \exp\left\{-\frac{1}{2}\left(\frac{\hat{S}_{xy}^{tot} - \sum_j S_{0_j}}{[\sum_j (S_{0_j}\sigma_j)^2]^{1/2}}\right)^2\right\}. \tag{3.7}$$

The expected value of the estimator $\hat{S}_{xy}^{tot}$ is thus the sum of the true densities S_{0_j}, and the variance of $\hat{S}_{xy}^{tot}$ is the sum of the variances of the density estimators $\hat{S}_{xy}(f_j)$.

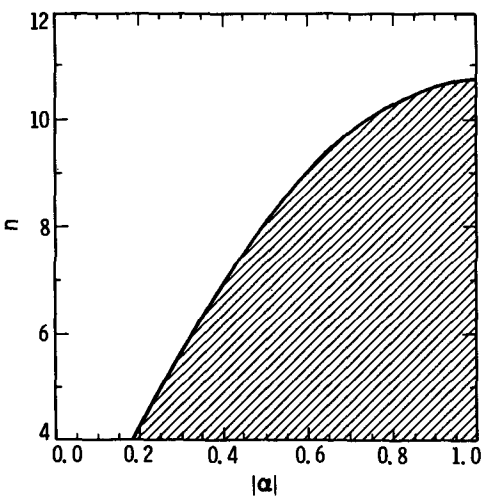

FIG. 4. Plot of the χ^2 statistic vs $|\alpha|$ and n for the differences between $p(\tilde{C})$ and a Gaussian. The χ^2 statistic is used as a measure of the normalized deviation between the two density functions. The hatched area denotes the region of $(n, |\alpha|)$ space for which the hypothesis that $p(\tilde{C})$ is a Gaussian would be violated at the 95% significance level.

4. Implications for experiment design

This section incorporates the statistical results derived above into a strategy for the design, from the standpoint of sampling, of S_{xy} measurement systems. The design of a system to measure $S_{xy}(f)$ or S_{xy}^{tot} requires compromises between a host of competing requirements and capabilities. We do not discuss the important issues related to the accuracies of the direct measurements themselves or the accuracies of sea-surface slopes estimated using finite-difference techniques (e.g., see the discussion in appendix B of Higgins et al., 1981). Instead, we use field data to illustrate the sensitivities of flux and flux density estimates to both sampling parameters and the shape of the true spectrum $S_{xy}(f)$.

The true cospectrum, $C(f)$, plays a central role in determining the accuracies of $\hat{S}_{xy}(f)$ and $\hat{S}_{xy}^{tot}$. The frequency resolution (and hence the basic record length T) of the data must be chosen so that the true cospectrum is approximately constant within each frequency band. Failure to achieve the required resolution results in biased estimates of the cospectrum (Jenkins and Watts, 1968) and violates assumptions fundamental to Goodman's derivation of (2.1).

Once the elementary bandwidth is established, the remaining choice is the total record length or, equivalently, the degrees of freedom $2n$. Criteria for choosing n depend strongly on the applications intended for the measurements. In all cases, however, knowledge of the spectrum $S_{xy}(f)$ is helpful in determining required n.

Consider, as a first example, the case where it is necessary to measure $S_{xy}(f)$ at a single frequency or at each of several frequencies, with an accuracy R defined such that

$$R = \mathrm{sd}[\hat{S}_{xy}(f)/S_{xy}(f)] = \{\mathrm{var}[\hat{S}_{xy}(f)]\}^{1/2}. \tag{4.1}$$

The standard deviation (sd) of the measurements $\hat{S}_{xy}(f)$ is a monotonically decreasing function of $|\alpha|$ for fixed n, as shown by Fig. 3. The critical bands, therefore, are those for which $|\alpha|$ will be a minimum. Figure 5a, derived from Fig. 3, shows the required n as a function of $|\alpha|$ for several values of the parameter R. Small values of R, corresponding to measurements with little (normalized) statistical variability, obviously require large values of n (i.e., long total record lengths). For flux density measurements to have a normalized standard deviation of 25%, one must have $n = 200$ for $|\alpha| = 0.2$, corresponding to a record length of 7.1 hours (assuming $\Delta f = 0.0078$ Hz). Figure 5a shows that the required total record length drops off rapidly as $|\alpha|$ increases.

In the absence of any information regarding the true spectrum $S_{xy}(f)$, the best that can be achieved is to pick a sampling period arbitrarily that is as long as possible. If this is done, the experimenter can still es-

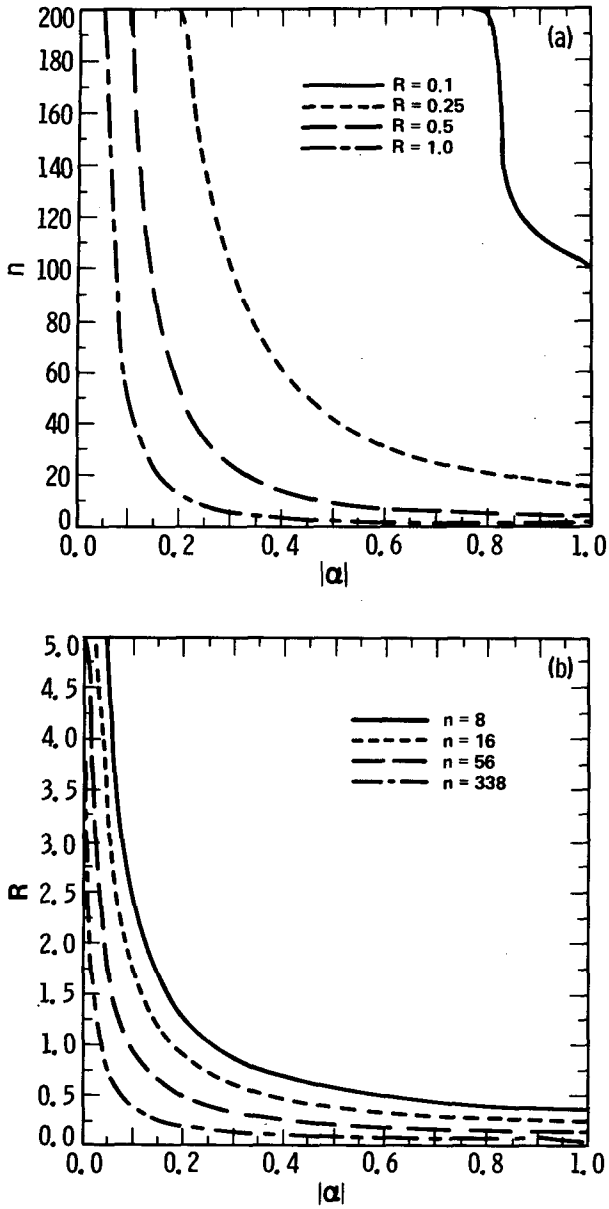

FIG. 5. (a) Plot of n vs $|\alpha|$ for four values of the normalized standard deviation. In order to estimate $S_{xy}(f)$ with high relative accuracy, n must be large (corresponding to long total record lengths). (b) R as a function of $|\alpha|$ for n = 8, 16, 56 and 338.

timate a priori the accuracy of the system as a function of conditions, using (2.8). The results of such a calculation are shown in Fig. 5b for sampling periods of 17.1 min, 34.2 min, 2 h, and 12 h (again, assuming Δf = 0.0078 Hz). Not surprisingly, for bands with small $|\alpha|$, even very long total record lengths result in relatively inaccurate estimates of $\hat{S}_{xy}(f)$.

Estimation of S_{xy}^{tot} is of great importance to coastal engineers, who use it for predicting accumulation of sediment in harbors and depletion of sand from beaches. Seymour and Castel (1985) and Coastal Data Information Program (1975) describe attempts to compile S_{xy}^{tot} climatologies at selected sites, using arrays that measure sea-surface elevation slopes. Using the results of section 3, the accuracy of individual estimates $\hat{S}_{xy}^{tot}$ can be assessed, and rational sampling parameters for such long-term measurement systems can be derived. In the previous example of $S_{xy}(f)$ estimation, the value of $|\alpha|$ in the frequency band of interest was seen to play a pivotal role in the accuracy of the estimator $\hat{S}_{xy}(f)$. The situation becomes even more complex for estimation of S_{xy}^{tot}. As shown by (3.7), the statistics of $\hat{S}_{xy}^{tot}$ depend both on the normalized variability of each density estimator $\hat{S}_{xy}(f)$ in the whole wind–wave frequency band, and on the actual shape of the $S_{xy}(f)$ spectrum across the wind–wave band. In other words, the statistics of $\hat{S}_{xy}^{tot}$ are the result of delicate interactions between normalized quantities [i.e., $|\alpha(f)|$] and unnormalized quantities [i.e., $S_{xy}(f)$]. It is not sufficient to know merely the approximate expected value of S_{xy}^{tot}, nor is knowledge of either the spectrum $\alpha(f)$ *or* the spectrum $S_{xy}(f)$ sufficient. Furthermore, since wave conditions at most sites vary significantly over time scales of days to months, the design of S_{xy}^{tot} measurement systems to meet a priori accuracy requirements is practically impossible.

Nonetheless, (3.7) can be used to predict the performance of a given sampling scheme for various hypothesized wave conditions. In addition, the dependence of the accuracy of the system on the sampling parameter n can be evaluated for an ensemble of hypothesized conditions, thus facilitating trade-off studies at the design stage.

Field data acquired by a slope array are used here to illustrate these points. Details of the array design and data reduction can be found in Gable (1981). The array was located in about 10 meters of water off Santa Barbara, California. Data presented here were acquired on 4 February, 14 February, and 15 February 1980, during the National Sediment Transport Study field experiment (Gable, 1981). For the purposes of this illustration, all data are assumed to be exact; that is, we take the mean measured values $\hat{\alpha}(f)$ and $\hat{S}_{xy}(f)$ to be the "true" values $\alpha(f)$ and $S_{xy}(f)$ in order to define our realistic (but hypothetical) wave conditions. In all three datasets, the waves had approximately the same significant height (total variance of sea-surface elevation was about 475 cm^2 in 10 m depth for each dataset), although Fig. 6a shows that the spectral distribution of wave energy varies somewhat from dataset to dataset. More striking variations between datasets are seen in the spectra of α (Fig. 6b) and S_{xy} (Fig. 6c). All waves in the frequency band 0.05–0.3 Hz were approaching the beach from the same quadrant on 4 February, leading to positive values of $\alpha(f)$ and $S_{xy}(f)$ at all frequencies. S_{xy}^{tot} is relatively large for this dataset, at 53 $\times$ 10^3 g s^{-2}.

Values of $\alpha(f)$ and $S_{xy}(f)$ are similarly positive for frequencies less than about 0.125 Hz on 15 February.

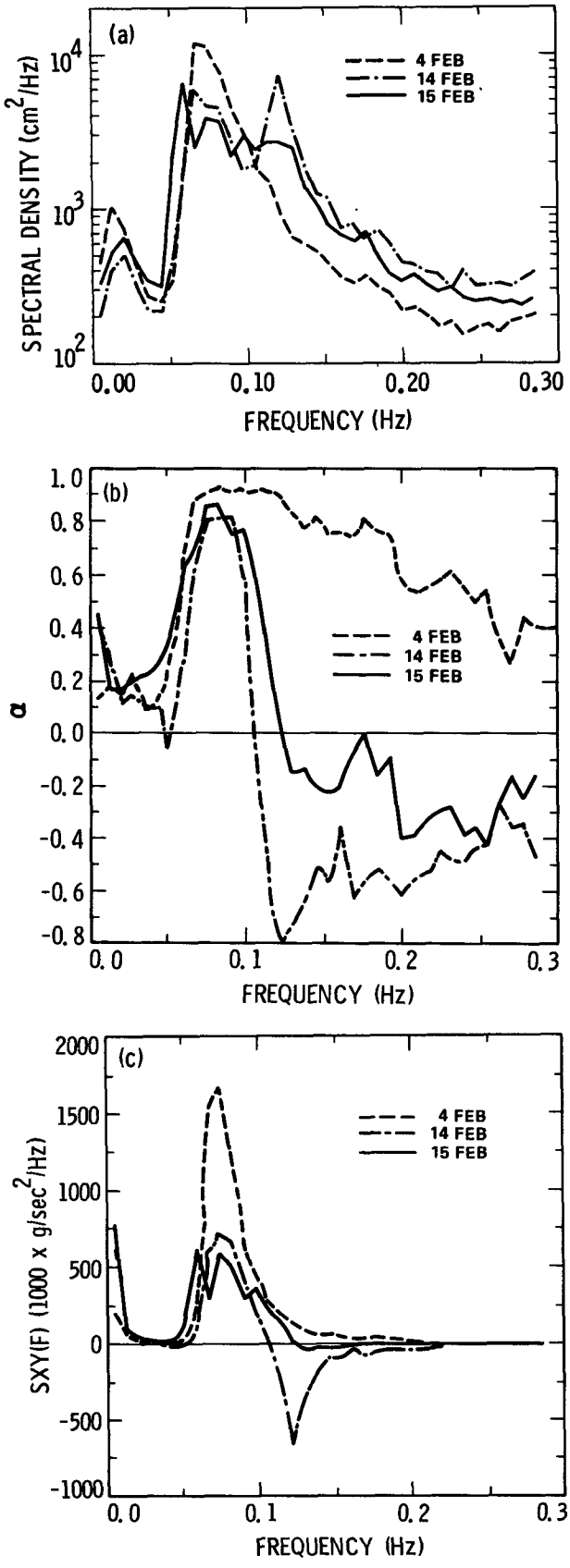

FIG. 6. (a) Spectra of sea-surface elevation for the Santa Barbara field data. (b) Spectra of α (normalized cospectrum) for the field measurements. (c) $S_{xy}(f)$ for the field data.

At higher frequencies, the waves were approaching from the opposite quadrant, leading to negative values of $\alpha(f)$ and $S_{xy}(f)$. The small magnitudes of $\alpha(f)$ and $S_{xy}(f)$ at these frequencies contributed little to the total momentum flux, which was 23×10^3 g s^{-2}. On 14 February, low-frequency waves ($\leq$0.10 Hz) contributed positive $S_{xy}(f)$, while large, higher-frequency waves contributed negative $S_{xy}(f)$, leading to a nearly balanced situation with small (5×10^3 g s^{-2}) total flux of longshore momentum.

We use the $\alpha(f)$ and $S_{xy}(f)$ data in Figs. 6b and 6c to calculate the performance of the $\hat{S}_{xy}^{\text{tot}}$ estimator as a function of n ($20 \leq n \leq 300$) for these conditions. Since we take $n > 11$, the Gaussian approximation to the true statistics is valid (see section 3), and (3.7) can be used. Absolute estimates of

$$\text{sd}[\hat{S}_{xy}^{\text{tot}}] = (\text{var}[\hat{S}_{xy}^{\text{tot}}])^{1/2} \tag{4.2}$$

are shown in Fig. 7a as functions of n. With a fixed bandwidth of 0.0078 Hz, $n = 20$ corresponds to a total data record length of about 42 min, while $n = 300$ corresponds a length of about 10.6 h. Standard deviations fall rapidly with increasing n for $n \leq 100$. For larger n, the curves flatten considerably. For all n, standard deviations are largest for the 4 February data, and smallest for the 15 February data.

It is instructive to examine normalized standard deviations

$$\text{sd}(\hat{S}_{xy}^{\text{tot}}/S_{xy}^{\text{tot}}) = \text{sd}(\tilde{S}_{xy}^{\text{tot}}) = (\text{var}[\tilde{S}_{xy}^{\text{tot}}])^{1/2} \tag{4.3}$$

because of the large variations in S_{xy}^{tot} between datasets. Figure 7b presents such data as a function of n for each dataset. Although the 4 February data have the largest absolute standard deviation (Fig. 7a), Fig. 7b shows that they have the smallest normalized deviation (i.e., the greatest relative accuracy). This is a direct consequence of the fact that the true $S_{xy}(f)$ values all have the same sign, and thus the true S_{xy}^{tot} [in the denominator in Eq. (4.3)] takes its maximum value. The 14 February data, on the other hand, have $S_{xy}(f)$ values that are both positive and negative, leading to a small magnitude for S_{xy}^{tot}. Thus, the normalized standard deviations are large for this dataset. The 15 February data are similar to 4 February, in that $S_{xy}(f)$ values with large magnitudes all have the same sign. Typically, existing S_{xy} measurement systems acquire data for about 68 min day^{-1} (four measurement periods of about 17 min each). Assuming stationary wave conditions so that all four measurement periods can be combined to form a daily average, the resulting $\hat{S}_{xy}^{\text{tot}}$ estimates would have a relative accuracy of about 7.5% (1σ) for 4 February, 9% (1σ) for 15 February, and 51% (1σ) for 14 February.

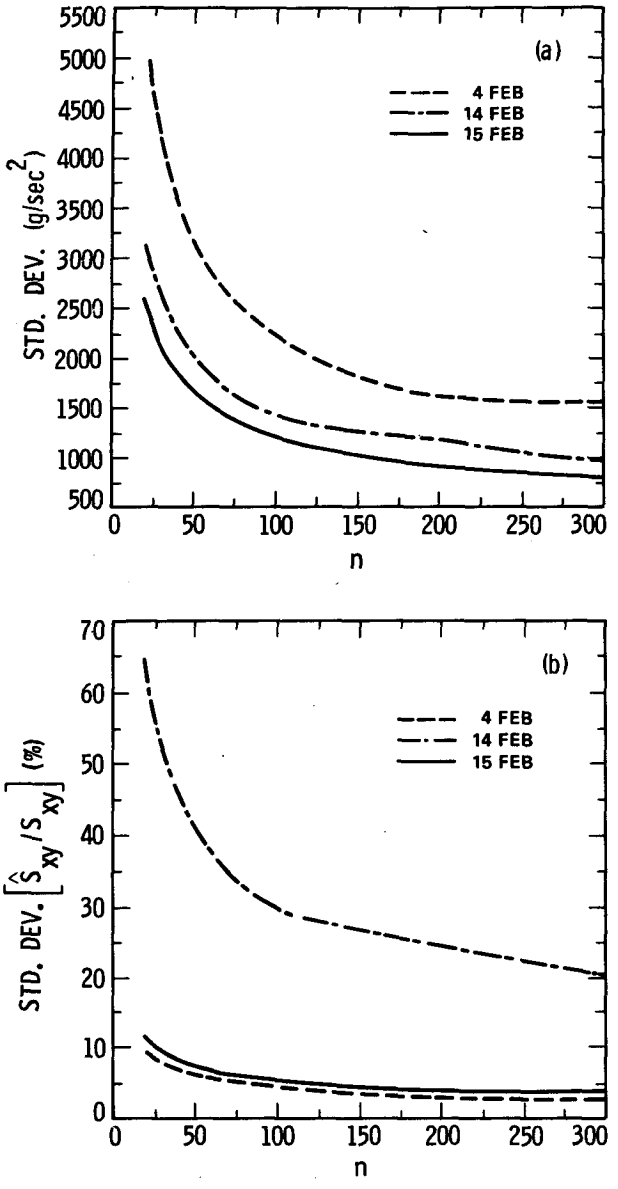

FIG. 7. (a) Standard deviations of S_{xy}^{tot} as a function of n for the data of Fig. 6. (b) As in (a) except normalized standard deviations (sd[$\hat{S}_{xy}^{tot}/S_{xy}^{tot}$]).

5. Maximum likelihood estimation of $S_{xy}(f)$

Previous sections have considered the statistics of momentum flux estimates, given some a priori knowledge of the true values. The population statistics can be used to design and evaluate sampling schemes, as illustrated in section 4. In this section we briefly describe an a posteriori method for estimating true values (and uncertainties) based on a limited set of data. Our method is a straightforward application of maximum likelihood inference as described, for example, in Jenkins and Watts (1968).

Knowledge of the functional form of the sampling pdf is central to the method of maximum likelihood inference. Briefly, the method involves substitution of the measured values into the sampling pdf, resulting in a "likelihood function" in which the unknowns are the "true" values (i.e., the "parameters" in the sampling distribution). Those values of the true parameters that maximize the likelihood function are the "maximum likelihood" estimates. The ratio of likelihoods (for two different sets of parameter values) quantitatively corresponds to the relative probability of one set of parameters being correct (as opposed to the other set). Integrals of the likelihood function about the maximum likelihood values can thus be used to estimate confidence intervals for the maximum likelihood estimates.

In principle, therefore, estimates of the spectral and cospectral values $\hat{A}$, $\hat{B}$, $\hat{C}$ and $\hat{D}$ can be substituted into the full joint pdf (2.1), resulting in a likelihood function for the true values A, B, C and D (or, alternatively, A, B, α and β). We will report the results of such analyses, using data from orthogonal-component measuring systems, in Freilich and Guza (in preparation).

In the present paper, however, we examine the simpler (albeit somewhat artificial) problem of estimating true cospectral [or $S_{xy}(f)$] values, assuming that the true autospectral values A and B are known, and that the true quadrature spectrum, D, is identically zero. The appropriate sampling pdf is thus given by (2.3), with the measured value $\hat{C}$ (or $\hat{\alpha} = \hat{C}/\sqrt{\hat{A}\hat{B}}$) known, and the true cospectrum C (or $\alpha = C/\sqrt{AB}$) as the unknown parameter. Note that α appears in (2.3) implicitly though the term δ [see (2.2)].

Recasting (2.3) as a likelihood function for α, and assuming $\sqrt{AB} = \sqrt{\hat{A}\hat{B}}$, one obtains

$$L(\alpha) = \left[\frac{n^{n+1/2}|\hat{\alpha}|^{n-1/2}}{\delta^{1/2}\Gamma(n)}\right] \exp\left\{\frac{2n\hat{\alpha}\alpha}{\delta}\right\} K_{n-1/2}\left(\frac{2n|\hat{\alpha}|}{\delta}\right). \quad (5.1)$$

Since likelihood values are unknown to within a multiplicative constant (i.e., only relative likelihoods have meaning), a term $2/\sqrt{\pi\hat{A}\hat{B}}$ has been dropped from (5.1).

Figure 8 presents $L(\alpha)$ for various values of $\hat{\alpha}$ and n. Note that all likelihoods in Fig. 8 have been normalized so that the maximum likelihood value for a given ($\hat{\alpha}$, n) combination is one. For small values of $|\hat{\alpha}|$, the likelihood functions are nearly symmetric about the maximum values. However, for $|\hat{\alpha}|$ near 1, the functions are somewhat asymmetric and skewed, with long tails extending toward low values of $|\alpha|$. This effect is most notable for small n.

Table 2 quantitatively presents important parameters corresponding to the likelihood functions of Fig. 8. Both the maximum likelihood estimates and the mean likelihood estimates are shown for each likelihood function. The mean likelihood estimate is given by

$$\bar{\alpha} \equiv \int_{-1}^{1} \alpha L(\alpha) d\alpha \Big/ \int_{-1}^{1} L(\alpha) d\alpha. \quad (5.2)$$

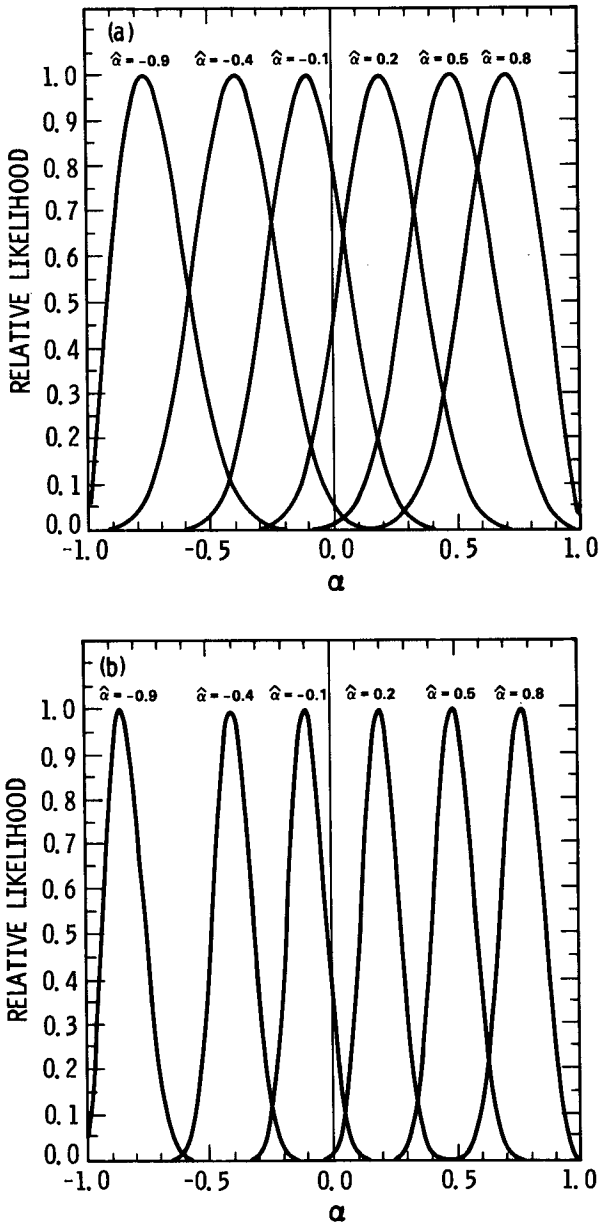

FIG. 8. Likelihood functions $L(\alpha)$ [see (5.1)] for measured values $\hat{\alpha} = -0.9, -0.4, -0.1, 0.2, 0.5$ and 0.8. All likelihood functions have been normalized such that the maximum likelihood is 1. (a) $n = 20$; (b) $n = 100$.

In the case of a likelihood function that is symmetric about its maximum value, the mean likelihood and maximum likelihood estimates will of course be identical. The data of Table 2 shows that this is approximately the case for all $|\hat{\alpha}|$ for n large, and for small and moderate $|\hat{\alpha}|$ even for n as small as 20. Mean and maximum likelihood estimates differ for large $|\hat{\alpha}|$ and small n, because of the somewhat asymmetrical shape of the likelihood function in this region of parameter space. Since the mean likelihood estimate takes account of the shape of the likelihood function over the full domain (while the maximum likelihood estimate does not), it is recommended that the mean likelihood estimate be used (Jenkins and Watts, 1968). In most cases of interest (moderate n and low-moderate $|\hat{\alpha}|$), however, there is no appreciable difference between the two estimates.

Maximum (or mean) likelihood estimates can differ from the measured values $\hat{\alpha}$. For the problem of interest here, this effect is most apparent for small n and large $|\hat{\alpha}|$. For parameters in this range, maximum likelihood estimates are lower (in magnitude) than the measured $|\hat{\alpha}|$. The physical interpretation of this result is that the measured $|\hat{\alpha}|$ most probably came from the high-value "tail" of a sampling distribution with lower $|\alpha|$. This is consistent with the sampling distributions shown in Fig. 1, where broader distributions are associated with smaller values of $|\alpha|$.

On the basis of calculations such as those illustrated in Fig. 8, it appears reasonable to approximate the likelihood function (5.1) by a Gaussian with the same mean and variance (Jenkins and Watts, 1968). This assumption allows approximate confidence limits (based on the percentage points of the normal distribution) to be calculated directly from the best-fit parameters. As the number of degrees of freedom associated with the measurements increases, the measured values $\hat{\alpha}$ become increasingly reliable (Table 2), and thus the likelihood functions become narrower for larger n (Fig. 8). In addition, the widths of the normalized likelihood functions, as approximated by the variance

$$\text{var}[\alpha] = \int_{-1}^{1} \alpha^2 L(\alpha) d\alpha - \left[\int_{-1}^{1} \alpha L(\alpha) d\alpha\right]^2, \quad (5.3)$$

are nearly independent of $\hat{\alpha}$. Equivalently,

$$\sigma^2 = \text{var}[\alpha]/\hat{\alpha}^2 \equiv \gamma/\hat{\alpha}^2, \quad (5.4)$$

TABLE 2. Parameters of the likelihood functions shown in Fig. 8. $\hat{\alpha}$ is measured normalized co-spectrum; α_m is maximum likelihood value; $\bar{\alpha}$ is the mean of the likelihood function; sd is the standard deviation of the likelihood function; sd/$\bar{\alpha}$ is normalized standard deviation (given in %); (7.5:1) are the values of α corresponding to likelihood values down by a factor of 7.5 from the maximum likelihood (if the likelihood function is Gaussian, these values correspond to the 95% confidence limits).

n	$\hat{\alpha}$	α_m	$\bar{\alpha}$	sd	sd/$\bar{\alpha}$	(7.5:1)
20	−0.9	−0.76	−0.72	0.14	19	(−0.98, −0.43)
20	−0.4	−0.39	−0.39	0.16	41	(−0.72, −0.06)
20	−0.1	−0.10	−0.10	0.15	153	(−0.42, 0.22)
20	0.2	0.20	0.20	0.16	78	(−0.12, 0.52)
20	0.5	0.48	0.48	0.16	34	(0.14, 0.81)
20	0.8	0.71	0.68	0.15	21	(0.37, 0.97)
100	−0.9	−0.85	−0.84	0.07	9	(−0.98, −0.68)
100	−0.4	−0.40	−0.40	0.08	19	(−0.56, −0.24)
100	−0.1	−0.10	−0.10	0.07	71	(−0.25, 0.05)
100	0.2	0.20	0.20	0.07	36	(0.05, 0.35)
100	0.5	0.50	0.50	0.08	16	(0.34, 0.66)
100	0.8	0.77	0.77	0.08	10	(0.37, 0.97)

where, to first order, γ is a function only of n. Figure 9 shows the approximate dependence of σ^2 on n.

6. Conclusions

We have examined the statistics of $\hat{S}_{xy}(f)$ and $\hat{S}_{xy}^{\text{tot}}$ derived from orthogonal-component measurement systems, using as a basis the statistics of cospectral estimates derived by Goodman (1957, 1963). The statistics of $\hat{S}_{xy}(f)$ and $\tilde{S}_{xy}(f) = \hat{S}_{xy}(f)/S_{xy}(f)$ were found to depend on both the true cospectral density $C(f)$ and the true normalized cospectral density $\alpha = C(f)/\sqrt{A(f)B(f)}$. Simple a priori estimates of the accuracy of a measurement system or sampling scheme are thus not possible, since the statistics of the measured quantities depend on the true values (which are beyond the control of the experimenter) as well as on the sampling scheme (over which the experimenter *does* have control). Physically, the normalized cospectral density α is a measure of the directional spread of the waves at the frequency of interest, with $|\alpha| = 1$ corresponding to a plane wave. The cospectral density itself, $C(f)$, is related both to the amplitudes of the waves and to the mean angle at which they are approaching the beach.

A simple, closed-form solution for arbitrary moments of $p[\tilde{S}_{xy}(f)]$ was obtained. Not surprisingly, the variance of $\tilde{S}_{xy}(f)$ decreases for increasing degrees of freedom $2n$, and for increasing true values $|\alpha|$ (Fig. 3). While the variance of $\hat{S}_{xy}(f)$ decreases dramatically with n for n small, little decrease with n was seen for $n \geq 40$, for all values of $|\alpha|$.

Given the probability density function (pdf) for flux density estimates $\hat{S}_{xy}(f)$, an expression for $p(\hat{S}_{xy}^{\text{tot}})$ was obtained using characteristic functions. A very simple but accurate approximation to the exact pdf was derived by noting that $p[\tilde{S}_{xy}(f)]$ is very nearly Gaussian for $n \geq 11$, independent of $|\alpha|$. The approximate pdf for $\hat{S}_{xy}^{\text{tot}}$ thus is itself Gaussian, with its mean and variance dependent on the summed means and variances of the density estimates $\hat{S}_{xy}(f)$ [cf. (3.7)].

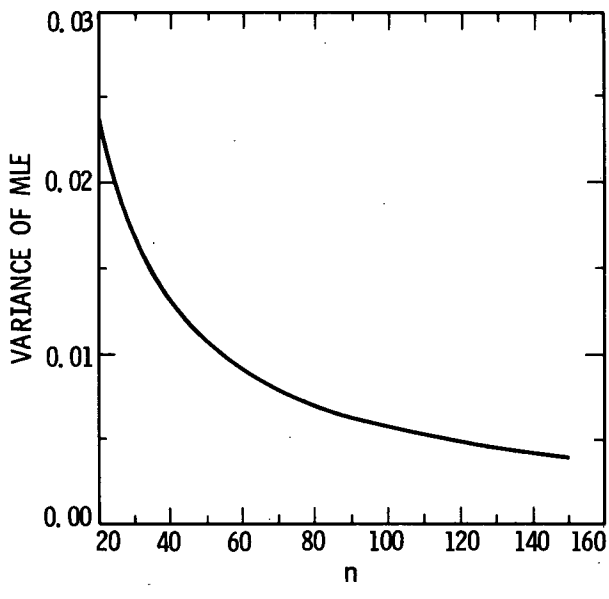

FIG. 9. Variance of the likelihood estimates of α as a function of n.

Examples, based on actual field measurements, were used to determine the performances of several sampling schemes and to illustrate the difficulties facing the experiment designer. In the examples, a fixed sampling scheme in which data is obtained for 68 min day^{-1} was shown to allow estimation of S_{xy}^{tot} with a relative accuracy of a few percent under conditions of nearly unidirectional waves approaching the beach from a large angle. However, the same sampling scheme resulted in only 51% (1σ) relative accuracy when the momentum fluxes associated with waves from different frequencies and directions nearly cancelled.

After measurements are taken, the sampling pdf's derived in sections 2 and 3 can be recast as likelihood functions for the true auto- and cross-spectral values. Although in practice the full joint pdf (2.1) should be used, the technique was illustrated for the simpler problem of estimating C (or α) alone. Likelihood functions were found to be nearly symmetric for all α and all n, and thus could be accurately approximated as Gaussian. This approximation allows quantitative uncertainties (error bars) to be assigned directly to the likelihood estimates. The uncertainties are functions of the sampling distribution and the actual measurements. To first order, the uncertainties depend only on the sampling parameter n and are independent of $|\alpha|$.

Recognition of the statistical nature of S_{xy} estimates is crucial for the proper design and interpretation of field measurements. Variance of flux estimates due to rather short (68 min day^{-1}) sampling periods may contribute significantly to the apparent "episodicity" of transport observed by Seymour and Castel (1985), although true day-to-day variations in wave conditions clearly also play an important role. Guza and Thornton (1978) remark on the "noisiness" of $\hat{S}_{xy}(f)$ and $\hat{S}_{xy}^{\text{tot}}$ measurements and corresponding (but apparently uncorrelated) variations in measured longshore currents in the surf zone. The results of the present paper provide a proper context for evaluating the "noisiness" of similar field measurements, in order to determine quantitatively whether the cause of the measured variability is strictly statistical, or whether the measurements imply that the statistics of the wave field are varying on some intermediate time scale (i.e., "nonstationarity" over the measurement interval).

Finally, we note that our results are applicable to measurements of many processes dependent on the cross spectrum between two (basically Gaussian) time series. Specifically, estimates of turbulent fluxes in the atmospheric surface layer are often obtained by calculating directly the mean product $\langle u'w' \rangle$, where u'

and w' are the fluctuating components of horizontal and vertical velocity (e.g., measured from aircraft using gust probes or at fixed points in space using sonic anemometers). The maximum likelihood technique briefly described in section 5 could be used to make estimates of the statistical accuracy of the measured/estimated fluxes.

Acknowledgments. This research was carried out at the Jet Propulsion Laboratory, California Institute of Technology, under contract with the National Aeronautics and Space Administration, and at the Center for Coastal Studies, University of California, San Diego. Until his death, support for S.S.P. was provided by the Office of Naval Research, Code 422CS (Coastal Sciences), under Contract N00014-75-C-0300. We wish to thank R. T. Guza for the Santa Barbara slope array data and for many helpful discussions, and T. H. C. Herbers for a critical reading of portions of the manuscript.

REFERENCES

Abramowitz, M., and I. E. Stegun, 1972: *Handbook of Mathematical Functions.* Dover, 1046 pp.

Bendat, J. S., and A. G. Piersol, 1971: *Random Data: Analysis and Measurement Procedures.* Wiley & Sons, 407 pp.

Borgman, L. E., 1976: Statistical properties of fast Fourier transform coefficients computed from real-valued, covariance-stationary, periodic random sequences. Tech. Paper No. 76-9, Coastal Eng. Res. Cen., U.S. Army Corps of Eng., Fort Belvoir, VA, 64 pp.

——, R. L. Hagan and T. Kuik, 1982: Statistical precision of directional spectrum estimation with data from a tilt-and-roll buoy. Topics in Ocean Physics, *Soc. Ital. Fis.,* Bologna, 418–438.

Bowen, A. J., 1969: The generation of longshore currents on a plane beach. *J. Mar. Res.,* **75,** 206–225.

Coastal Data Information Program, 1975–: Monthly Summary Reports. Inst. of Mar. Resources, University of California, San Diego. Reports are numbered sequentially from No. 1, dated Dec. 1975.

Gable, C. G., 1981: Report on data from the NSTS experiment at Santa Barbara, California, Jan–Feb 1980. IMR Ref. No. 81-5, Inst. of Mar. Resources, University of California, San Diego, 314 pp.

Goodman, N. R., 1957: On the joint estimation of the spectra, cospectrum, and quadrature spectrum of a two-dimensional stationary Gaussian process. Scientific Paper No. 10, Engineering Statistics Laboratory, New York University, 168 pp.

——, 1963: Statistical analysis based on a certain multivariate complex Gaussian distribution (an introduction). *Ann. Math. Stat.,* **34,** 152–177.

Guza, R. T., and E. B. Thornton, 1978: Variability of longshore currents. *Proc. 16th Coast. Eng. Conf., ASCE,* Hamburg, 756–775.

Haubrich, R. A., 1965: Earth noise, 5 to 500 millicycles per second. *J. Geophys. Res.,* **10,** 944–952.

Higgins, A. L., R. J. Seymour and S. S. Pawka, 1981: A compact representation of ocean wave directionality. *Appl. Ocean Res.,* **3,** 105–112.

Jenkins, G. M., and D. G. Watts, 1968: *Spectral Analysis.* Holden-Day, 525 pp.

Kinsman, B., 1965: *Wind Waves.* Prentice-Hall, 676 pp.

Komar, P. D., and D. L. Inman, 1970: Longshore sand transport on beaches. *J. Mar. Res.,* **75,** 5914–5927.

Long, R. B., 1980: The statistical evaluation of directional spectrum estimates derived from pitch/roll buoy data. *J. Phys. Oceanogr.,* **10,** 944–952.

Longuet-Higgins, M. S., 1970a: On the longshore currents generated by obliquely incident sea waves, 1. *J. Geophys. Res.,* **75,** 6778–6789.

——, 1970b: Longshore currents generated by obliquely incident sea waves, 2. *J. Geophys. Res.,* **75,** 6790–6801.

——, and R. W. Stewart, 1964: Radiation stresses in water waves: A physical discussion with applications. *Deep-Sea Res.,* **11,** 529–562.

Pawka, S. S., 1982: Wave directional characteristics on a partially sheltered coast. Ph.D. dissertation, University of California, 246 pp.

——, D. L. Inman and R. T. Guza, 1983: Radiation stress estimators. *J. Phys. Oceanogr.,* **13,** 1698–1708.

Seymour, R. J., and A. L. Higgins, 1977: A slope array for measuring wave direction. *Proc. Workshop on Coastal Processes and Instrumentation,* La Jolla, University of California, San Diego Sea Grant Publ. No. 62, IMR Ref. No. 78–102, 133–142.

——, and D. Castel, 1985: Episodicity in longshore sediment transport. *J. Waterway, Port, Coast Ocean Eng.,* **111.**